9-25-2017

Orientation Dependent Compression Behavior of $Co_{35}Ni_{35}Al_{30}$ Single Crystals

Peizhen Li
University of Kentucky, peizhen.li@uky.edu

Haluk E. Karaca
University of Kentucky, karacahaluk@uky.edu

Yury I. Chumlyakov
Tomsk State University, Russia

Orientation Dependent Compression Behavior of $Co_{35}Ni_{35}Al_{30}$ Single Crystals

Notes/Citation Information
Published in *Journal of Alloys and Compounds*, v. 718, p. 326-334.

Digital Object Identifier (DOI)
https://doi.org/10.1016/j.jallcom.2017.04.307

Orientation Dependent Compression Behavior of $Co_{35}Ni_{35}Al_{30}$ Single Crystals

Peizhen Li [1], Haluk E. Karaca [1], Yury I. Chumlyakov[2]
[1] Department of Mechanical Engineering, University of Kentucky, Lexington, Kentucky 40506-0503, USA
[2] Siberian Physical-Technical Institute, Tomsk State University, Tomsk 634050, Russia.

Abstract

The shape memory effect (SME) and superelasticity (SE) behavior of homogenized $Co_{35}Ni_{35}Al_{30}$ single crystals were systematically characterized along the [100], [110] and [111] orientations under compression. The shape memory behavior of CoNiAl was found to be highly orientation and stress/temperature dependent. Maximum compressive recoverable strains were 3.98 % in [110], 3 % in [100] and 0.30 % in [111] orientations, respectively. The $Co_{35}Ni_{35}Al_{30}$ demonstrated a very high superelastic temperature window of more than 350 °C along the [100] and [110] orientations. Moreover, two-way shape memory effect with very low thermal hysteresis of about 6 °C was observed along the [110] orientation. The large decrease of recoverable strain and hysteresis with stress (or temperature) was mainly attributed to the difference of elastic moduli of transforming phases.

Keywords: Shape memory alloys; CoNiAl; Single crystal; Two-way shape memory effect; superelasticity

1. Introduction

The magnetic shape memory alloys (MSMAs) received considerable attention since they have the ability to show large reversible magnetic field-induced strains (MFIS) [1, 2]. There are two main mechanism for reversible shape change: variant reorientation as in NiMnGa alloys or phase transformation as in NiMnCoIn alloys [3-5]. Although NiMnGa Heusler alloys can achieve high MFIS with low magnetic field, their extreme brittleness restricts their envisioned applications as magneto-actuators, sensors, caloric materials or energy harvesters. CoNiGa [6-9] and CoNiAl [10-12] alloys were developed as an alternative MSMA and they demonstrated high strength, stable behavior, low stress for variant reorientation, ability to alter transformation temperatures with heat treatments and high resistance to oxidation. The ductility of Co-based alloys were found to be improved mainly due to the existence of γ-phase (disordered fcc A1) [13]. The stress required for the onset dislocation slip of CoNiAl has been reported around 1100

MPa [11]. Comparing to other MSMAs, CoNiAl alloys have relatively inexpensive constituents and their transformation and Curie temperatures can be altered by composition alteration [14].

It is well known that shape memory response of SMAs are highly temperature, stress and orientation dependent [15, 16]. Temperature dependent superelastic response of CoNiAl polycrystals were studied under compression where two stage phase transformation was observed at room temperature with superelastic strain of 4 % [11]. The orientation dependent behavior of CoNiAl single crystals were studied and it has been found that transformation strain is highly orientation dependent, a large superelastic temperature window of more than 150 °C can be observed in [100] orientation and there is huge tension-compression asymmetry [10, 11, 17, 18]. Moreover, it was revealed that transformation strain decreases with stress and temperature [10] [19]. The [100]-oriented $Co_{35}Ni_{35}Al_{30}$ single crystals were studied as a function of temperature under compressive loading in solutionized and trained (cyclic loading) state conditions [20]. It was reported that training results in austenite stabilization and strengthening, and consequently increase the amount of stress induced martensite which is attributed to the formation of fine coherent precipitates during training. Several studies suggested that the morphology of precipitates and inter-particle spacing influence the martensitic transformation, where the large inter-particle spacing (100-400nm) and surrounding stressed region in the case of CoNiAl alloys [18, 21] favor the nucleation of martensite, raising the M_s temperature. During superelasticity, a pronounced decrease of transformation strain with temperature was reported in CoNiGa along the [100] orientation [22] which demonstrates a large superelastic window of more than 385 °C. The decrease in superelastic strain attributed to the single variant formation at low temperature and the formation of multiple variants at high temperature. Although the mechanical characterization in terms of thermal cycling and superelastic behavior of CoNiAl alloys have been reported under compression and tension [10, 11, 17, 23, 24], orientation and temperature dependent shape memory behavior of CoNiAl alloys have not been systematically studied.

The present study was undertaken on the shape memory and superelasticity behavior of $Co_{35}Ni_{35}Al_{30}$ (at %) single crystals along the [100], [110] and [111] orientations systematically. The composition of $Co_{35}Ni_{35}Al_{30}$ was selected to have a low martensite start temperature for easy single crystal growth [14] and observe superelasticity at room temperature for practical

applications. The current study also presents the theoretical transformation strain calculations of CoNiAl single crystals for compression. For CoNiAl alloys, B2 austenite has a lattice parameter of a_0=0.287$\dot{A}$, and $L1_0$ martensite has lattice parameters of a=0.385$\dot{A}$ and c=0.314$\dot{A}$ [10]. The three orientations are selected due to the following facts: the activation of slip systems in B2 phase is difficult in [100] orientation upon loading due to inhibition of the active slip systems of [100] <001> and [110] <001>, [25-27], and the transformation strain is large in [110] orientation and very low in [111] orientation.

2. Experimental Procedure

CoNiAl alloy was cast to a nominal composition of Co-35Ni-30Al in at. %. Single crystals were grown by using the Bridgman technique in a He atmosphere. The composition of single crystal was determined to be Co-35.32Ni-27.69Al (at. %) using a Zeiss EVO MA 10 scanning electron microscope (SEM) equipped with an energy dispersive X-Ray spectroscopy (EDX) microanalysis system. Compression samples (4mm x 4mm x 8mm) were cut using electro-discharge machining (EDM) such that their compression axes are along the [100], [110] and [111] directions in B2 phase. Specimens were initially homogenized at 1350 °C for 6 hours in sealed quartz tubes filled with argon and followed by water-quenching at room temperature. CoNiAl single crystal alloys present a single B2 phase at room temperature after annealing and it transforms into a tetragonal $L1_0$ martensite phase. The transformation temperatures of the two-phase alloy were determined by using Perkin-Elmer Pyris 1 differential scanning calorimetry (DSC) with thermal cycling rate of 10 °C min^{-1}. Mechanical experiments were conducted using an MTS Landmark servohydraulic test frame equipped with customized compression and tension grips. The applied force was controlled by a 100 kN capable load cell (precision: $\pm$ 0.1 N), and the axial strains were measured with a high-temperature MTS extensometer. The heating/cooling of the samples was achieved by conduction through compression plates at the rates of 10 °C min^{-1} during heating and -5 °C min^{-1} during cooling by using a PID driven Omega CN8200 series temperature controller.

3. Results

In this section, the compressive response of CoNiAl single crystals will be revealed along the selected orientations. Two types of experiment were carried out; 1) thermal cycling under

constant load and 2) stress cycling at constant temperature. Two-way shape memory effects were also revealed in [100] and [110] orientations.

3.1.Shape Memory Effect

Figure 1 shows the DSC response of homogenized $Co_{35}Ni_{35}Al_{30}$ single crystal. It is clear that during transformation, sharp peaks were observed in CoNiAl alloys. It should be noted that in NiTi alloys the transformation peaks are broader and smoother [28-30]. Upon cooling, martensite start (M_s) and finish (M_f) temperatures were -44.3 °C and -66.6 °C, respectively. As seen in Figure 1, the transformation was quick initially, leading to high and sharp peaks. Further cooling resulted in a gradual type transformation with small peaks. Upon heating, austenite start (A_s) and finish (A_f) temperatures were -31.3 °C and 10.3 °C, respectively. These sharp/narrow peaks indicate "burst type" transformation where the quick and sequential formation/ disappearance of martensite plates were observed during thermal cycling.

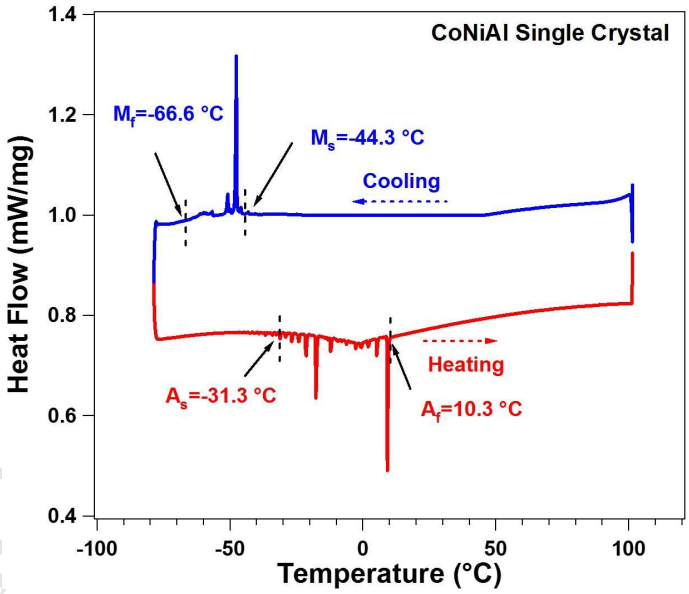

Figure .1. DSC response of a homogenized $Co_{35}Ni_{35}Al_{30}$ single crystal.

$Co_{35}Ni_{35}Al_{30}$ single crystals were thermally cycled under selected stress levels to determine their shape memory effects and their responses at selected stress levels are shown in Figure 2. The maximum applied stress level was 300 MPa for [100] and [110] orientations, and 800 MPa for [111] orientation. The compressive stress (σ) was isothermally applied when the

material was in the austenitic phase at a temperature beyond A_f, and then the sample was cooled down to below M_f and heated back to above A_f under constant stress. In [100], the phase transformation was gradual and the difference between M_f and M_s was large, indicating large elastic energy storage [31]. However, it seems there are two types transformation during cooling where the type I shows relatively sharp behavior than the type II shown in Figure 2a. Here, type I behavior is defined as the burst type phase transformation region while the type II is the graduate phase transformation after burst transformation. Intersection method was used to determine the strains of these two transformation regions as shown in Figure 3a. The transformation temperatures increased with applied stress, where the M_s and A_f were -40 °C and -10 °C under 25 MPa and increased to 109 °C and 149 °C under 300 MPa, respectively. A detail schematic in Figure 3a shows how to determine the total strain (ε_{SME}^{t}) and irrecoverable strain (ε_{SME}^{irr}). ε_{SME}^{t} was determined at M_s and ε_{SME}^{irr} was measured as the difference between the cooling and heating curves at temperature above A_f +20 ºC. The ε_{SME}^{rec} was calculated as the difference between ε_{SME}^{t} and ε_{SME}^{irr}. Temperature hysteresis was determined graphically at the midpoint of the total strain, and measured by the temperature differences between the heating and cooling curves. Figure 3b is used to determine the compressive superelastic strain at plateau region (ε_{SE}^{p}) and under zero stress (ε_{SE}^{0}) graphically, as well as the Young's moduli of austenite and martensite phases. The critical stress (σ_c) was determined by using the intersection method shown in Figure 3b. ε_{SME}^{rec} was initially increased with stress from 1.53 % under 25 MPa to 3 % under 75 MPa, and then decreased to 2.18 % under 200 MPa. Thermal hysteresis initially increased and then decreased with stress, and a small amount of ε_{SME}^{irr} of 0.2 % was observed under 300 MPa.

The thermal cycling response along the [110] orientation in Figure 2b is similar to the behavior of [100] where the transformation temperatures increased with applied stress. ε_{SME}^{rec} increased with stress up to 50 MPa and then decreased with further increase in stress. The maximum ε_{SME}^{rec} of [110] was 3.96 % under 50 MPa, higher than what was observed in [100] orientation. Thermal hysteresis increased to the maximum value of 91.7 ºC at 25 MPa and then decreased with stress. ε_{SME}^{irr} of 0.18 % was observed under 75 MPa. Under low stress (<100MPa), burst type transformation was observed where the sample suddenly transformed from austenite to martensite (type I). At high stresses (>100 MPa), combined type I+II transformation was observed where the sudden transformation was followed by gradual change in strain. The type I

(ε_{SME}^{I}) and type II (ε_{SME}^{II}) strains were determined by using the method shown in Figure 3a. The total stain is the sum of those two strains. The type I+II behavior in [100] and [110] can also be correlated to the DSC response where the burst type transformation was followed by an incremental transformation.

Figure 2c shows the thermal cycling response of [111] orientation. The transformation strain was very low, of about 0.3 % under 300 MPa. Almost negligible ε_{SME}^{irr} of 0.05 % was observed under high stress of 800 MPa. The behavior was very stable and almost stress independent as the transformation temperatures and ε_{SME}^{rec} did not increase significantly with stress. Thermal hysteresis increased from 16 °C under 100 MPa to the maximum value of 20 °C under 300 MPa, and then decreased with stress. As seen in Figure 2c, incremental transformation behavior was observed at all stress levels.

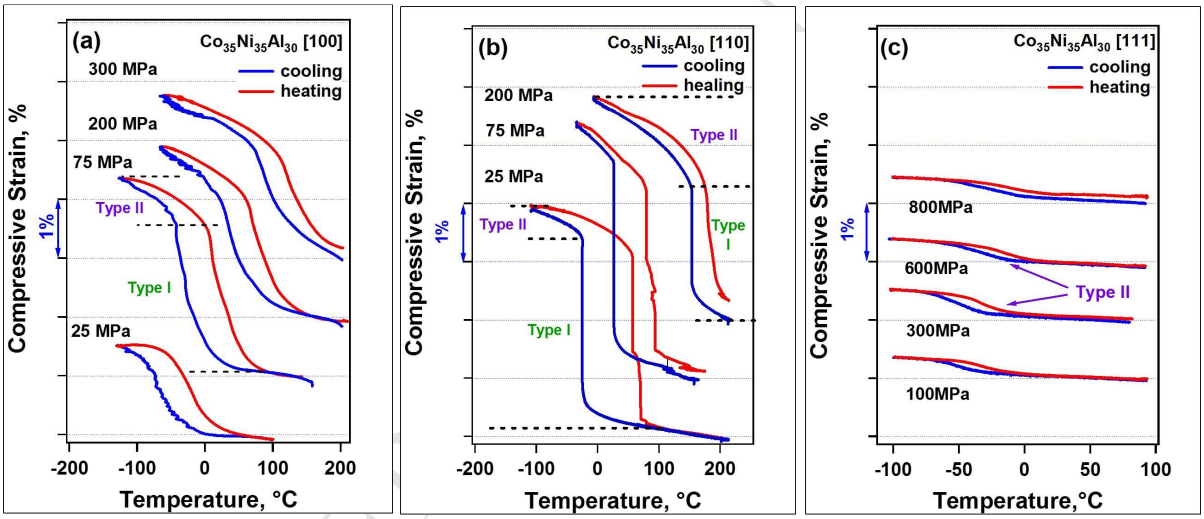

Figure. 2. Thermal cycling responses of the homogenized $Co_{35}Ni_{35}Al_{30}$ alloys along the a) [100] b) [110] and c) [111] orientations under selected compressive stress.

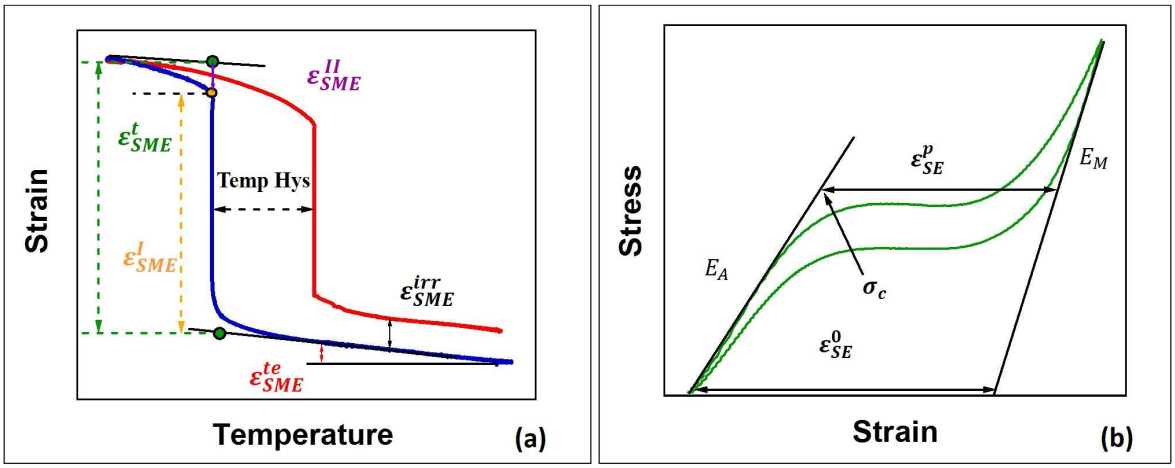

Figure. 3. Schematic of strain calculation from a) SME and b) superelasticity.

3.2.Two-way Shape Memory Effect

After thermal cycling under compressive stress responses shown in Figure 2, an additional thermal cycling was conducted under a low compressive stress of 5 MPa along the [100] and [110] orientations to explore the TWSME. The thermal cycling compression responses before and after "training" along the [100] and [110] orientation are shown in Figures 4a and 4b, respectively. In [100], the two-way shape memory strain (ε_{TWSME}) was increased from 0.33 % to 2.85 % with training, which is almost equal to the maximum strain observed during thermal cycling responses shown in Figure 2a. Moreover, two-stage transformation behavior was observed. In [110], two-way shape memory strain was increased from 0.34 % (before training) to 3.58 % (after training) with a very narrow thermal hysteresis of 6.8 ºC. The ε_{SME}^{I} strain was measured as 2.83 % along the [110] orientation. The low temperature hysteresis indicates the good compatibility of transforming phases and it is desired for actuator applications. M_s was determined as -67 ºC from Figure 1. After training, M_s increased in both orientations to 0 ºC for [100] and 26 ºC for [110]. However, after training, A_f was 25 ºC for [100] and 28 ºC for [110], which is close to the A_f of 10.3 ºC (determined from Figure 1). The increase of M_s with training can mainly be attributed to i) the internal stress created during thermal cycling under high stress and ii) the generation of plastic strain and residual stresses during thermal cycling experiments shown in Figure 2. These two factors may help the nucleation of martensite, increasing compatibility and enhancing strength, leading to the increase of M_s and decrease of dissipation energy. Detail discussion can be found in the phase diagram section.

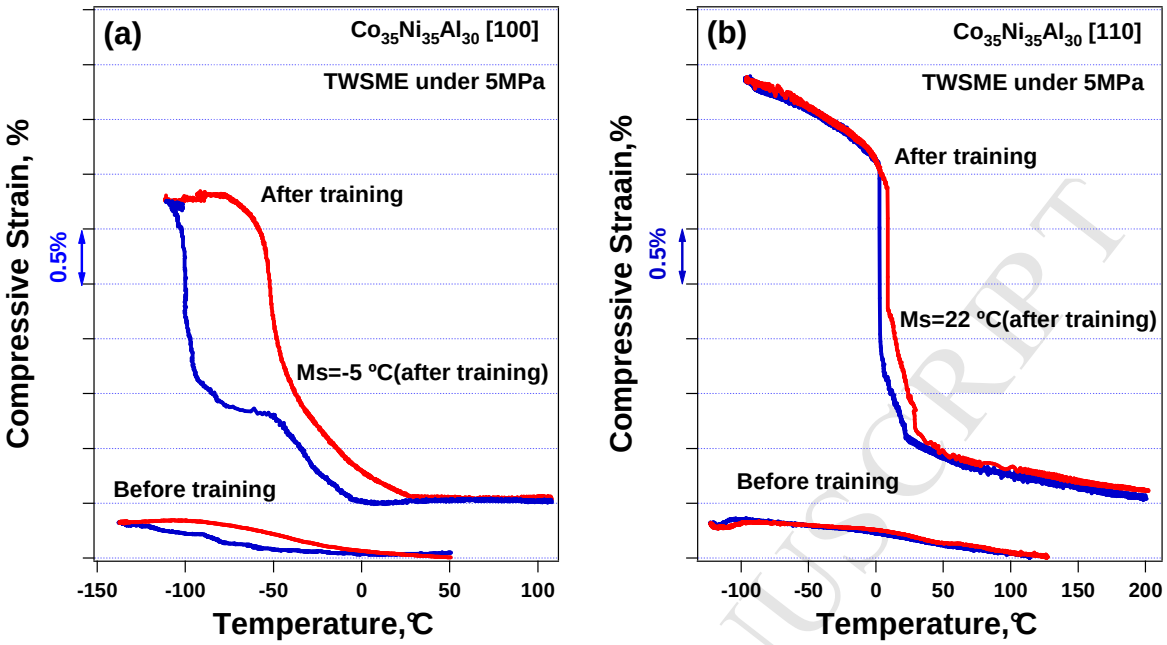

Figure. 4. Compressive two-way shape memory effect behavior of $Co_{35}Ni_{35}Al_{30}$ single crystal before training under 5 MPa and after training under 5 MPa with orientation of a) [100] and b) [110].

3.3.Superelasticity

Figures 5a shows the selected temperature dependent superelastic response of [100] oriented single crystal in compression. The superelastic response was determined from 0 ºC to an elevated temperature of 350 °C. The single crystal of [100] was first loaded to a total strain of 4 % and then unloaded at a constant temperature 0 ºC. Almost perfect shape recovery was observed upon unloading. Then, the temperature was increased by 20 ºC up to 100 ºC and 50 ºC afterwards where the loading/unloading was repeated isothermally. Perfect superelastic behavior was observed for a very large temperature window of 350 ºC. The critical stress for phase transformation was increased while transformation strain was decreased with temperature. Figure 5a clearly showed a strong temperature dependent superelastic behavior. The slope during the transformation (m_{tr}) was low at low temperatures (< 40 ºC), and increased with temperature. This behavior can be attributed to the increased difficulty for phase transformation and detwinning [32]. Moreover, the results are in good agreement with the incremental shape memory behavior observed in Figure 2a. The stress hysteresis was 41 MPa at 80 °C and substantially increased to 181 MPa at 350 °C. Perfect superelasticity was observed at 350 °C with maximum stress level reaching to 1.2 GPa. A large superelasticity window of 350 °C was revealed along the [100]

orientation which is more than two times larger than what was reported before for CoNiAl alloys [11] and similar to CoNiGa alloys [22].

Figure 5b shows the superelastic response along the [110] orientation with a temperature interval of 20 ºC. The sample was firstly loaded up to a total strain of 4 % at 57 ºC. After the initial linear elastic behavior, a clear transformation occurred with a plateau like response at low temperatures (<137 ºC). At higher temperatures, m_{tr} increased considerably. At 57 ºC, there were three notable features: 1) very low stress hysteresis of about 16 MPa; 2) perfect superelasticity where the unloading path followed similar behavior with loading curve; 3) stress dropped two times during forward transformation and increased two times during back transformation. The stress required for phase transformation increased with testing temperatures. The decrease of stress in plateau region is related to burst type behavior observed in shape memory effect test. Since SE tests were conducted under strain control, the decrease of stress is detected. If force control was used instead of strain control, it would show a burst type transformation behavior at the plateau region similar to ones observed at force controlled SME tests. Stress hysteresis increased dramatically from 16 MPa at 57 ºC to 250 MPa at 307 ºC. Perfect superelasticity was observed till 307 °C. At higher temperatures, small irrecoverable strain was detected. At high temperature of 407 ºC, with a 2 % strain deformation, maximum stress was reached to 1.2 GPa and perfect superelasticity was again attained with large stress hysteresis. The SE temperature window of [110] was found to be higher than 350 °C. Moreover, high strength for plastic deformation (>1200 MPa) was revealed in both [100] and [110]

The transformation strain at the plateau region of SE decreased with temperature. Such a behavior can be attributed to the formation of multiple variants which enhanced the variant-variant interaction at high temperature [22] and change in lattice parameters with temperature. The methods used to determine Young's modulus of austenite (E_A) and martensite (E_M), and transformation strain under stress at plateau region (ε_{SE}^{p}) and under zero stress (ε_{SE}^{0}) were shown in Figure 3b. The highest SE recoverable stain was about 3.4 % for the temperature range of 57-137 °C, indicating the fewer martensite variants growth at low temperature. However, the recoverable strain reduced pronouncedly to about 0.7 % between 207-407 °C and it is attributed to the growth of multiple variants at high temperature.

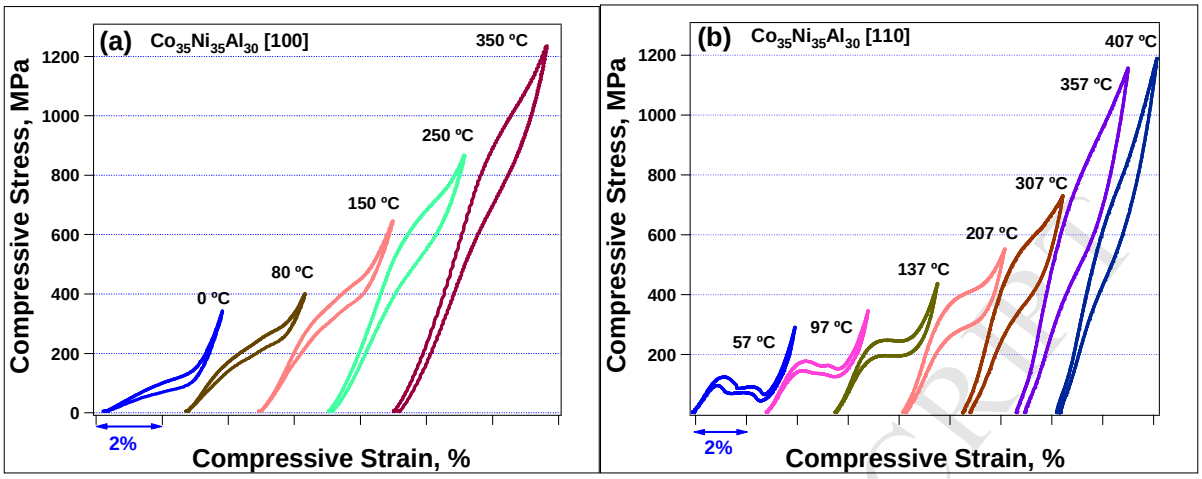

Figure. 5. Compressive stress-strain responses along the a) [100] and b) [110] orientations as a function of testing temperature.

4. Discussion

4.1.Elastic Modulus

Figure 6 shows the elastic moduli during loading and unloading for [100] and [110] orientations as a function of temperature, extracted from the results shown in Figure 5. Initial elastic regions during loading and unloading were used to determine the moduli of austenite (E_A) and martensite (E_M), respectively. It should be noted that at low temperatures, the end of plateau and the elastic region where modulus of martensite obtained was clear. However, at higher temperatures, it is not clear if the transformation is fully completed. At high temperatures the modulus determined during unloading might have contributions from austenite, thus, the modulus during unloading was marked as E_M*. It should be noted that the modulus of conventional materials such as Al, Cu, Ti decrease with increasing temperature due to the material softening [33-35]. The modulus of shape memory alloys shows a highly temperature dependence behavior. Temperature dependence of the elastic constants and anisotropy factors were reported in NiTi-based alloys [36-38], where elastic constants decreases prior to the forward martensitic transformation, mainly due to the softening. Similar softening was also observed in magnetic NiMnGa alloys [39, 40]. For B2 crystals there exist three elastic constants moduli (c_{11}, c_{12}, c_{44}) where c' ((c_{11}-c_{12})/2) and anisotropy factor A (c_{44}/c') are two important factors in martensitic transformation. As shown in Figure 6, E_A and E_M* have similar trends where their moduli decreased with decreasing temperature for both orientations prior to the martensitic transformation. The E_M* in [100] decreased with temperature below 80 ºC and then it

increased with temperature. The increase of E_M* at higher temperatures can be attributed to the change in lattice parameters with stress and temperature, incomplete transformation and multivariant martensite formation. At all orientations, elastic modulus was higher during unloading when it is compared to the elastic modulus during loading. At 100 ºC, the modulus of martensite was three times higher than the modulus of austenite in [110] orientation. It should be noted that E_A is higher than E_M in NiTi alloys [41].

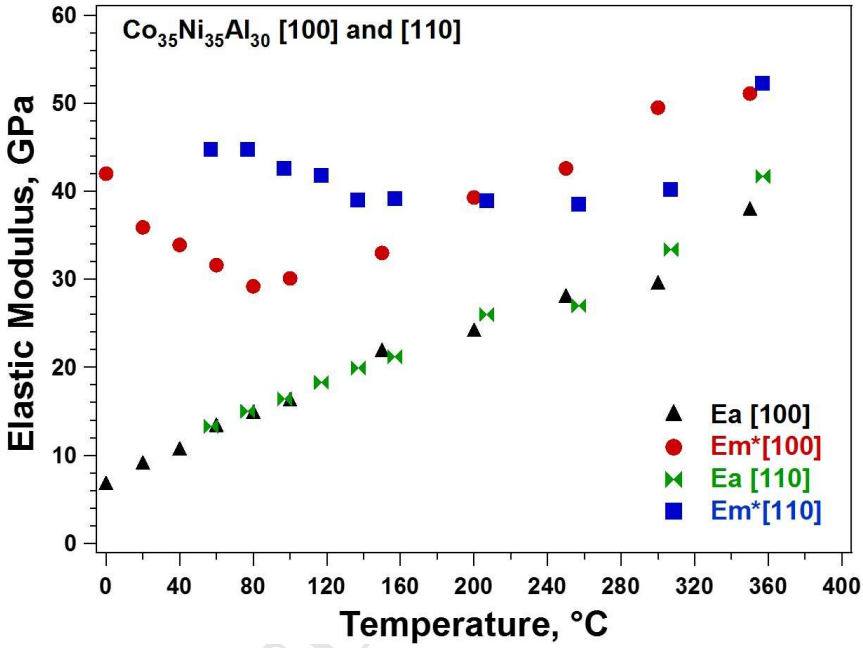

Figure. 6. Young's modulus of austenite and martensite as a function of temperature in [100] and [110] orientations. Elastic moduli during initial loading and unloading were extracted from Figure 5 by using the schematic in Figure 3b.

4.2.Transformation Strain

The ε_{SME}^{rec} were extracted from Figures 2, and plotted as a function of applied stress in Figure 7. It shows that ε_{SME}^{rec} for both the [100] and [110] orientations increases with applied stress at low stress region due to the increased volume fraction of favored martensite variants. The maximum ε_{SME}^{rec} were measured as 3 % at 75 MPa, 3.96 % at 50 MPa, and 0.3 % at 200 MPa along the orientation [100], [110], and [111], respectively. After the peak value, the recoverable strains decrease linearly with stress for all orientations. In [100] and [110] orientations, ε_{SME}^{rec} decrease from 3 % to 1.78 % and 3.96 % to 2.18 % when stress increases from 50 MPa to 300 MPa, respectively. The decrease in recoverable strain with stress or temperature can be attributed

to the large changes in lattice parameters and elastic moduli with temperature and the difference in Young's moduli of austenite and martensite phases.

It should be noted that at the plateau region, both austenite and martensite phases are compressed, thus they are elastically deformed. The difference between the ε_{SE}^{p} and ε_{SE}^{0} is increasing with the difference between the elastic moduli of transforming phases, as in CoNiAl alloys. ε_{SE}^{p} and ε_{SE}^{0} along the [100] and [110]orientations were plotted in Figure 7 by using the critical stress for transformation and temperature from superelasticity experiments shown in Figure 5. For both orientations, ε_{SE}^{p} and ε_{SE}^{0} decreased considerably with stress. The ε_{SE}^{p} is in good agreements with ε_{SME}^{rec} in both orientations, especially in [110] orientation. The ε_{SE}^{0} exhibits a relatively higher values than both $\varepsilon_{SE}^{p}\ and\ \varepsilon_{SME}^{rec}$ which can be attributed to difference in moduli of transforming phases. If the $\varepsilon_{SE}^{p}$is known, calculated superelastic strain under no stress (ε_{SE}^{0c}) can be obtained by the equation below:

$$\varepsilon_{SE}^{0c} = \varepsilon_{SE}^{p} + \left(\frac{\sigma_c}{E_A^T} - \frac{\sigma_c}{E_M^T}\right) \qquad (1)$$

Where E_A^T is the Young's modulus of austenite and E_M^T is the Young's modulus of martensite, and σ_c is the critical stress for phase transformation.

In [110] at 57 ºC, σ_c is 145 MPa, ε_{SE}^{p} is 2.91 %, E_A is 13.3 GPa and E_M is 44.7 GPa. Thus, the ε_{SE}^{0c} can be determined as 3.67 % which is higher than ε_{SE}^{p} of 2.91 % and close to the experimental measurement of ε_{SE}^{0} of 3.35 %. The error can attributed to inaccurate determination of ε_{SE}^{p} due to the lack of flat plateau region. Similar to the superelastic strain equation, the calculated SME strain under zero stress (ε_{SME}^{0c}) can be estimated as;

$$\varepsilon_{SME}^{0c} = \varepsilon_{SME}^{rec} + \left(\frac{\sigma}{E_A(T)} - \frac{\sigma}{E_M(T)}\right) \qquad (2)$$

Where σ is the applied constant stress, $E_A(T)$ and $E_M(T)$ are the elastic moduli of austenite and martensite, respectively, at the temperature where the ε_{SME}^{rec} was determined. ε_{SME}^{0c} for [100] and [110] orientations were added to Figure 7. It is clear that the ε_{SME}^{0c} is higher than the ε_{SME}^{rec} and the corrected strains have linear fit in both [100] and [110] orientations. Thus, ε_{SME}^{0c}at zero stress level is named as "projected strain" and shown in Figure 7. The projected strains of SME are

4.43 % and 4.85 % for [100] and [110] orientations, respectively. Furthermore, ε_{TWSME} , determined from the TWSME responses of [100] and [110] orientation shown in Figure 3, were added to Figure 7. It is worth to note that ε_{TWSME} is very close to the highest recoverable strains observed for both [100] and [110] orientations.

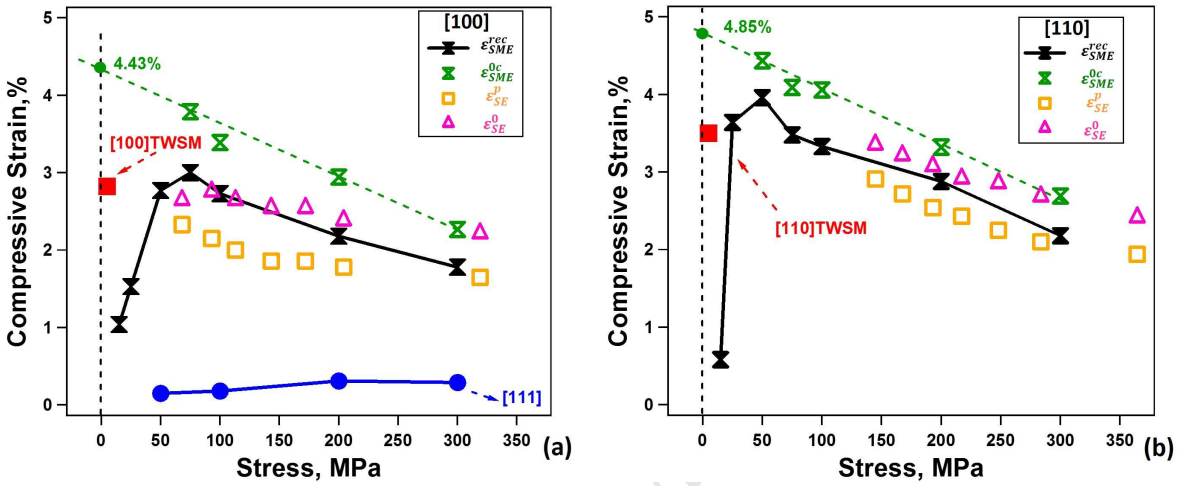

Figure. 7. The relationship of compressive strain vs. stress for three orientations a) [100] and [111], b) [110]. In detail, ε_{SME}^{rec} is the recoverable strain measured from SME under stress, ε_{SME}^{0c} is the corrected SME strain under zero stress, ε_{SE}^{p} is the strain measured from SE at plateau region, ε_{SE}^{0} is the strain measured from SE under zero stress.

Transformation strain is generated from the crystal structural difference between martensite and austenite phases. In this study, as shown by Figure 7, the degree of the change of strain with temperature in superelasticity and with stress in shape memory response are orientation dependent (the slope of the ε_{SME}^{rec} and stress were -4.41x10^{-3} %/MPa, -6.50 x 10^{-3} %/MPa for [100] and [110] , respectively, for the stress levels above 50 MPa), which had already been reported in Cobalt based alloys [10, 23]. However, it should be noted that the strain increases with temperature/stress in NiTi while it decreases in CoNiAl [29]. Combined with equation (1), a schematic is provided to explain the decrease in transformation strain with stress in Figure 8. The decrease in ε_{SE}^{p} in CoNiAl alloys along the [100] and [110] orientations is mainly due to fact that the E_A is considerable lower than E_M. In NiTi, the E_A is higher than E_M, resulting in increased ε_{SE}^{p} with stress as shown by the schematic in Figure 8b. It should be kept in mind that critical stress of transformation increases with temperature and elastic moduli of

transforming phases change with temperature as well. Thus, the combined effects of those two facts govern the change in ε_{SE}^{p}. In CoNiAl, the difference in elastic moduli of transforming phases is very high but σ_c is low at temperatures close to M_s. As temperature increases, the difference in elastic moduli of transforming phases decrease but σ_c increases. Thus, ε_{SE}^{p} is governed by those two competing facts. Lastly, it should be noted that in all cases the corrected recoverable strain decreases with temperature which can be attributed the change in lattice parameters.

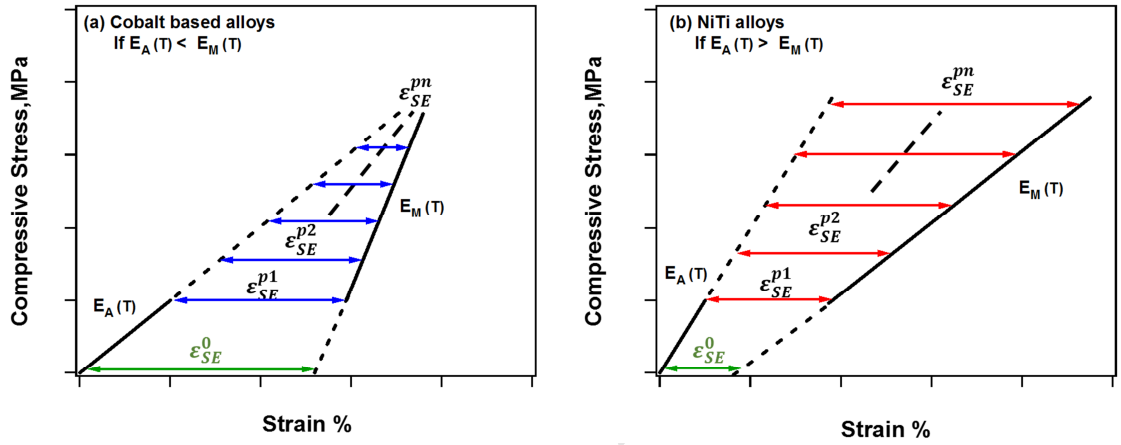

Figure. 8. A schematic of superelastic transformation strain at plateau region as a function of increasing stress. a) CoNiAl where $E_A < E_M$ and b) NiTi where $E_A > E_M$.

4.3.Phase Diagram

M_s of three orientations are extracted from Figure 2 and plotted as a function of applied stress in Figure 9. For all orientations, M_s increases with stress. Such a linear relation between stress and temperature is well explained by the Clusius-Clapeyron (C-C) relationship of;

$$\frac{\Delta\sigma(T)}{\Delta T} = -\frac{\Delta S}{\varepsilon_{tr}} = -\frac{\Delta H}{T_0 \varepsilon_{tr}} \qquad (3)$$

$\Delta\sigma(T)$ is the change in critical stress, ΔT is the change in temperature, ΔS is the specific or molar transformation entropy change and ΔH is the enthalpy change. T_0 is the equilibrium temperature that can be estimated in the usual form: $T_0 = \frac{1}{2}(M_s + A_f)$, and ε_{tr} is the transformation strain. From the SME experiments, C-C slopes were determined as 1.96 MPa $°C^{-1}$, 1.25 MPa $°C^{-1}$ and 22.80 MPa $°C^{-1}$ along the [100], [110] and [111] orientations, respectively. From the SME

experiments shown in Figure 2, the maximum ε_{SME}^{rec} are determined to be 3 %, 3.98 % and 0.3 % along the [100], [110] and [111] orientation, respectively. It is clear from equation (3) that C-C slope decreases with increased transformation strain when $\Delta H/T_0$ is constant which is the case for this study of CoNiAl single crystals. In [110], ε_{SME}^{rec} is highest and C-C slope is lowest. The maximum C-C slope of 22.8 MPa °C^{-1} was observed in [111] orientation, which also has the lowest ε_{SME}^{rec} of about 0.3 %. The conventional NiTi single crystals was reported to have C-C slopes of 4-8 MPa °C^{-1} in compression [42].

The critical stress for forward transformation as a function of temperature were extracted from Figure 5 and added to the Figure 9 for [100] and [110] orientations. The maximum σ_c in [110] orientation occurs at M_d where testing at higher temperatures results in plastic deformation and decrease in σ_c. Figure 9 shows that [100] orientation has a high strength of greater than 850 MPa and it is in good agreement with previous findings [19, 43, 44]. The superelasticity C-C slopes are 1.45 MPa °C^{-1} for [100] and 1.55 MPa °C^{-1} for [110] orientations. In [100] orientation, the superelasticity is observed from -20 to 350 °C as shown in Figure 9. In [110] orientation, the SE was observed from 57 °C to 407 °C. It is clear that in both orientation the SE is very large (~350 °C) which is due to their low CC slope and high strength. The high C-C slope of [111] orientation results in the lack of SE as σ_c increases rapidly with temperature and reaches to the critical stress for plastic deformation at temperatures above A_f.

According to the C-C slop from Eq (3), we can calculate the stress change ($\Delta\sigma$) between prior to the thermal cycling and after TWSME. As shown in Figure 1 and 4, the $\Delta M_s^{[110]}$= 25 °C-(-44°C) = 69 °C. Therefore, with SME C-C slop of [110] orientation, we have:

$$\Delta\sigma_{SME}^{[110]} = CC_{SME}^{[110]} * \Delta M_s^{[110]} = \frac{1.25MPa}{°C} * 69\,°C = 86.25\ \text{MPa}$$

Follow the same procedure for [100] orientation, we will get $\Delta\sigma_{SME}^{[100]} = 78.40MPa$. The observed stresses are the internal stress created during the thermal cycling experiments and can be the main reason account for the cause of M_s increase in TWSME.

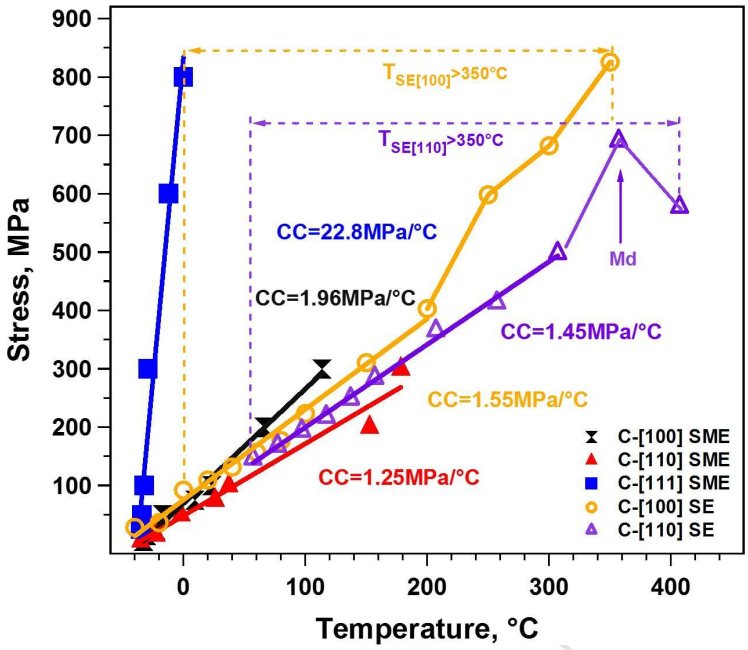

Figure. 9. Stress vs. temperature phase diagram of $Co_{35}Ni_{35}Al_{30}$ single crystals. Ms and σ_c are extracted from the load-biased thermal cycling (Figure 2) and superelastic tests (Figure 5), respectively, by using the schematics shown in Figure 3b.

4.4.Thermal and Stress Hysteresis

Figure 10 shows the thermal hysteresis of three orientations as a function of applied stress. The change in thermal hysteresis with stress has a similar trend as the recoverable strain, where the thermal hysteresis increase at low stress region and then decrease with stress. In Figure 10, thermal hysteresis of [100] orientation increases from 35.4 °C under 15 MPa to 54.2 °C under 50 MPa, and then decrease to 33.8 °C under higher stress of 300 MPa. The change in thermal hysteresis is more pronounced in [110] orientation, where it shows the sudden jump from 56.3 °C at 15 MPa to 91.7 °C at 25 MPa due to the burst type (Type I) phase transformation during thermal cycling experiments under low stress levels. The thermal hysteresis then decreases to its lowest value of 28.3 °C at 200 MPa, and then increases to 52.37 °C at 300 MPa. For [100] orientation, the transformation behavior happens gradually with a smooth transition at each stress level, indicating stored elastic energy. However, the transformation occurs in a very sudden manner at low stress levels in [110]. This burst type response indicates the absence of stored elastic energy where once the energy required for nucleation of martensite is achieved, a sudden

transformation is observed. The orientation dependence of thermal hysteresis can mainly be attributed due to the difference of elastic energy relaxed during forward transformation [10].

The effects of lattice parameters on the thermal hysteresis were reported before [45]. It was found that lattice parameters governs the compatibility between the transforming phases and thermal hysteresis. In CoNiAl single crystals, the large decrease of thermal hysteresis with temperature can be attributed to the effects of temperature and stress to lattice parameters and crystal structure that govern the compatibility of transforming phases. The increase in thermal hysteresis at high stress levels is due to the increased plastic strain and dissipation energy.

Thermal hysteresis obtained from the TWSME responses of [100] and [110] orientations are also displayed in Figure 10. It is notable that the thermal hysteresis reaches to an extreme low value of 6.7 °C along the [110] orientation under 5 MPa. Such narrow thermal hysteresis from TWSME can be understood by some defects such as that dislocation, stabilized martensite can modify nucleation and growing martensite of TWSME, and this martensite can be very fine compare with the initial created martensite.

It should be noted that $Co_{35}Ni_{35}Al_{30}$ alloys shows the lowest thermal hysteresis reported among Cobalt based SMAs. Low thermal hysteresis and large ε_{TWSME} make these alloys very promising for actuator applications

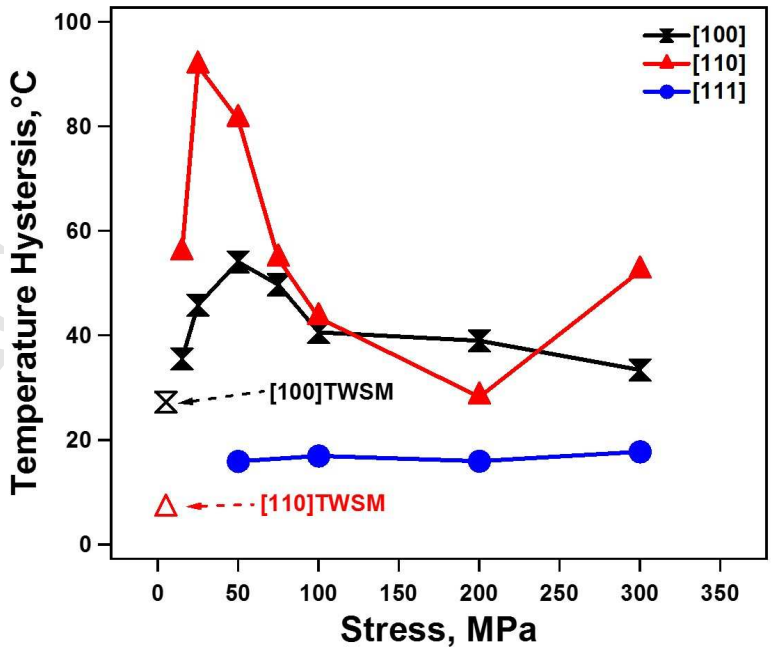

Figure. 10. The relationship of temperature hysteresis vs. stress for three orientations [100], [110], and [111].

Stress hysteresis can be extracted from Figure 5 for [100] and [110] orientations, where the stress hysteresis decreases with temperature. It is difficult to determine the stress hysteresis of [100] shown in Figure 5a due to the lack of plateau regions for both forward and backward transformations. As mentioned before, at low temperatures, stress decrease and increase abruptly during forward and backward transformation, respectively, in [110]. The observation of the first stress drop after reaching to the stress required for transforming phases was also observed in polycrystalline $Co_{38}Ni_{33}Al_{29}$ alloys at room temperature [11] and it is attributed to the differences between the stresses required for nucleation and propagation [11]. The first stress drop can also be attributed to the differences of the speed of the phase front and cross head motion [46], where the phase boundary moves faster than the cross head, resulting the stress drop. The second drop can be linked to the nucleation and propagation of another phase front and/or detwinning. The stress drop in superelasticity can be correlated with the responses observed during the thermal cycling experiments shown in Figure 2b. In [110], Type I (burst type) deformation was observed at low stress levels which corresponds to stress drops in Figure 5b at low temperatures. Eventually, thermal cycling under stress becomes Type I+II behavior at higher stress level in Figure 2b where in SE, stress drops are observed at low temperatures ($m_{tr}<0$) and single plateau is observed at mid temperatures ($m_{tr}\sim0$) and stress increased during transformation at higher temperatures ($m_{tr}>0$). To be noted, if force control was used instead of displacement control, burst type behavior would have been observed at lower temperatures during SE. The sudden phase transformation or stress drops are not observed in [100] to the extent observed in [110], however clearly, transformation was fast at first and then incremental with further cooling. Such differences between [100] and [110] can be stemmed from the formation of only twinned martensite along the [100] orientation and twinned and then detwinned martensite along the [110] orientation. The increase of stress hysteresis of both [100] and [110] orientations with temperature can be attributed to plastic deformation. As the critical stress for transformation increases with temperature, plastic deformation occurs and increases the dissipation energy and hysteresis

4.5. Theoretical Strain Calculation

The transformation strain of SMAs is governed by the crystal structure and lattice parameters of transforming phases. The theoretical transformation strain as a function of crystallographic orientation can be calculated by using the framework based on the "Energy Minimization Theory" [47, 48]. For CoNiAl alloys, B2 austenite has a lattice parameter of a_0=0.287*Å*, and $L1_0$ martensite has lattice parameters of a=0.385*Å* and c=0.314*Å* [10]. Table 1 includes the theoretical transformation strain calculations along the [100], [110], and [111] orientation for Correspondence Variant Pair (CVP) and detwinned martensite formation under no stress. CVP is the martensite plate which contains two compatible martensite variants. The theoretical calculation of CVP is the strain change caused by the formation of CVP during thermal cycling, while the detwinning is the growth of one variant within a martensite in expense of the other [49]. The detwinning produces additional recoverable strain, especially in tension. The maximum experimental recoverable strains observed in shape memory and superelastic tests are also listed, as well as the projected SME strain. As shown in Table 1, the experimental SME strains are very close to the maximum SE strains (under zero stress). The projected SME strains measured from Figure 7 are 4.43 % and 4.85 % for [100] and [110], respectively. In [100], although the experimental SME strain is lower than the theoretical strain due to the stress/ temperature effect, the projected SME strain (4.43 %) which is the corrected value at zero stress, closes to the theoretical number in both CVP (5.01 %) and Detwinned (5.01 %). It is hard to predict the transforming type by only comparing the experimental and theoretical strain values since they are very close. However, the inconspicuous type I+II behavior compared with [110] orientation shows that the transformation might have contributions from both CVP and Detwinned. In [110], the projected SME strain (4.85 %) almost equals to the theoretical Detwinned value (5.01) and the burst type strain (type I) is close to the theoretical CVP number (2.47 %), indicating the CVP and Detwinned transformations exist in [110] orientation. Moreover, the SME/SE experiment also shows those two types transformation profoundly at low stress/ temperature. The experimental SME strain in [111] is almost negligible compared with other two orientations, and it is reasonable when compare to theoretical strains.

Table. 1. Experimental recoverable strains from SME and SE, "projected SME" strains, theoretical strain calculations of CVP and detwinned martensite along the [100], [110], and [111] orientations.

	Experimental Strain (%)			Theoretical Strain (%)	
	SME	Projected SME	SE	CVP	Detwinned
[100]	3	4.43	2.75	5.01	5.01
	2.42 (Type I)				
[110]	3.98	4.85	3.35	2.47	5.01
	3.54 (Type I)				
[111]	0.31	0.31	NA	0.03	0.03

Conclusion

In this study, shape memory characteristics of $Co_{35}Ni_{35}Al_{30}$ (at %) alloy single crystals were investigated under compression. Transformation behavior under constant stress levels, and superelasticity as a function of strain and temperature were studied as well as two-way shape memory behavior. The conclusions can be listed below:

1. The shape memory behavior of CoNiAl alloys is highly orientation, stress and temperature dependent. The maximum compressive recoverable strains in $Co_{35}Ni_{35}Al_{30}$ single crystal oriented in [100], [110], and [111] are 3 %, 4 %, and 0.31 %, respectively. The recoverable strains decrease substantially with stress/temperature.
2. Perfect superelasticity is observed along the [100] and [110] orientations. Low stress hysteresis of 16 MPa is observed in superelasticity along the [110] orientation. The lack of SE in [111] orientation is attributed to the high C-C slope. The SME response of [111] orientation is stable and temperature independent.
3. The $Co_{35}Ni_{35}Al_{30}$ single crystal oriented in [100] and [110] have a large superelasticity window of more than 350 °C, thus CoNiAl alloys are promising candidates for high temperature applications. The burst type transformation behavior is observed in both [100] and [110] orientations. Applied stress affects the transformation behavior where both burst and gradual shape change are observed at high stress levels.
4. Two-way shape memory effect (TWSME) behavior with very low thermal hysteresis is observed in [100] and [110] orientations.
5. The decrease in recoverable strain during SE and SME tests is mainly attributed to the difference in Young's moduli of austenite and martensite phases.

6. Stress-temperature phase diagram under compression is constructed for $Co_{35}Ni_{35}Al_{30}$ single crystals. C-C slopes of 1.96 MPa/°C, 1.25 MPa/°C, 22.80 MPa/°C were obtained along the [100], [110] and [111] orientations, respectively.

Acknowledgments

This work was supported in part by the KSEF-148-502-15-355 and NSF CMMI-1538665 programs.

References

[1] K. Ullakko, J. Huang, C. Kantner, R. O'handley, V. Kokorin, Applied Physics Letters, 69 (1996) 1966-1968.
[2] A. Sozinov, A. Likhachev, N. Lanska, K. Ullakko, Applied Physics Letters, 80 (2002) 1746-1748.
[3] A.S. Turabi, H.E. Karaca, H. Tobe, B. Basaran, Y. Aydogdu, Y.I. Chumlyakov, Scripta Materialia, 111 (2016) 110-113.
[4] H.E. Karaca, I. Karaman, B. Basaran, Y. Ren, Y.I. Chumlyakov, H.J. Maier, Advanced Functional Materials, 19 (2009) 983-998.
[5] H.E. Karaca, I. Karaman, B. Basaran, Y.I. Chumlyakov, H.J. Maier, Acta Materialia, 54 (2006) 233-245.
[6] J. Liu, H. Xie, Y. Huo, H. Zheng, J. Li, Journal of alloys and compounds, 420 (2006) 145-157.
[7] J. Liu, H. Zheng, M. Xia, Y. Huang, J. Li, Scripta materialia, 52 (2005) 935-938.
[8] G. Liu, Z. Liu, X. Dai, S. Yu, J. Chen, G. Wu, Science and Technology of Advanced Materials, 6 (2005) 772-777.
[9] Y. Kishi, C. Craciunescu, M. Sato, T. Okazaki, Y. Furuya, M. Wuttig, Journal of magnetism and magnetic materials, 262 (2003) L186-L191.
[10] H. Karaca, I. Karaman, Y. Chumlyakov, D. Lagoudas, X. Zhang, Scripta materialia, 51 (2004) 261-266.
[11] H. Karaca, I. Karaman, D. Lagoudas, H. Maier, Y.I. Chumlyakov, Scripta materialia, 49 (2003) 831-836.
[12] K. Oikawa, T. Ota, F. Gejima, T. Ohmori, R. Kainuma, K. Ishida, Materials Transactions-JIM, 42 (2001) 2472-2475.
[13] R. Kainuma, M. Ise, C.-C. Jia, H. Ohtani, K. Ishida, Intermetallics, 4 (1996) S151-S158.
[14] K. Oikawa, T. Ota, F. Gejima, T. Ohmori, R. Kainuma, K. Ishida, Materials transactions, 42 (2001) 2472-2475.
[15] I. Kaya, H. Karaca, M. Souri, Y. Chumlyakov, H. Kurkcu, Materials Science and Engineering: A, (2017).
[16] S.M. Saghaian, H.E. Karaca, H. Tobe, M. Souri, R. Noebe, Y.I. Chumlyakov, Acta Materialia, 87 (2015) 128-141.
[17] R. Hamilton, H. Sehitoglu, C. Efstathiou, H. Maier, Y. Chumlyakov, X. Zhang, Scripta materialia, 53 (2005) 131-136.
[18] C. Efstathiou, H. Sehitoglu, A.W. Johnson, R. Hamilton, H. Maier, Y. Chumlyakov, Scripta materialia, 51 (2004) 979-985.
[19] Y.I. Chumlyakov, I. Kireeva, E.Y. Panchenko, E. Timofeeva, Z. Pobedennaya, S. Chusov, I. Karaman, H. Maier, E. Cesari, V. Kirillov, Russian Physics Journal, 51 (2008) 1016-1036.
[20] J. Dadda, H. Maier, I. Karaman, Y.I. Chumlyakov, Acta Materialia, 57 (2009) 6123-6134.

[21] D. Canadinc, J. Dadda, H.J. Maier, I. Karaman, H.E. Karaca, Y.I. Chumlyakov, Smart materials and structures, 16 (2007) 1006.
[22] J. Dadda, H. Maier, I. Karaman, H. Karaca, Y.I. Chumlyakov, Scripta materialia, 55 (2006) 663-666.
[23] D. Meyer, H. Maier, J. Dadda, I. Karaman, H. Karaca, Materials Science and Engineering: A, 438 (2006) 875-878.
[24] Y. Chumlyakov, E. Panchenko, I. Kireeva, I. Karaman, H. Sehitoglu, H. Maier, A. Tverdokhlebova, A. Ovsyannikov, Materials Science and Engineering: A, 481 (2008) 95-100.
[25] D. Miracle, Acta Metallurgica et Materialia, 41 (1993) 649-684.
[26] E. Hornbogen, G. Brückner, G. Gottstein, Zeitschrift für Metallkunde, 93 (2002) 3-6.
[27] N. Surikova, Y.I. Chumlyakov, Fizika Metallov i Metallovedenie, 89 (2000) 98-107.
[28] X. Zhang, H. Sehitoglu, Materials Science and Engineering: A, 374 (2004) 292-302.
[29] J.A. Shaw, S. Kyriakides, Journal of the Mechanics and Physics of Solids, 43 (1995) 1243-1281.
[30] J. Khalil-Allafi, A. Dlouhy, G. Eggeler, Acta Materialia, 50 (2002) 4255-4274.
[31] E. Acar, H.E. Karaca, B. Basaran, F. Yang, M.J. Mills, R.D. Noebe, Y.I. Chumlyakov, Materials Science and Engineering: A, 573 (2013) 161-165.
[32] K. Gall, J. Tyber, V. Brice, C.P. Frick, H.J. Maier, N. Morgan, Journal of Biomedical Materials Research Part A, 75 (2005) 810-823.
[33] J. Tallon, A. Wolfenden, Journal of Physics and Chemistry of Solids, 40 (1979) 831-837.
[34] M. Fukuhara, A. Sanpei, Journal of materials science letters, 12 (1993) 1122-1124.
[35] D.O. Thompson, D. Holmes, Journal of Applied Physics, 30 (1959) 525-541.
[36] X. Ren, N. Miura, K. Taniwaki, K. Otsuka, T. Suzuki, K. Tanaka, Y.I. Chumlyakov, M. Asai, Materials Science and Engineering: A, 273 (1999) 190-194.
[37] X. Ren, N. Miura, J. Zhang, K. Otsuka, K. Tanaka, M. Koiwa, T. Suzuki, Y.I. Chumlyakov, M. Asai, Materials Science and Engineering: A, 312 (2001) 196-206.
[38] K. Otsuka, X.B. Ren, in: Materials Science Forum, Trans Tech Publ, 2002, pp. 177-184.
[39] L. Dai, J. Cui, M.R. Wuttig, in: Smart Structures and Materials, International Society for Optics and Photonics, 2003, pp. 595-602.
[40] P. Zhao, L. Dai, J. Cullen, M. Wuttig, Metallurgical and Materials Transactions A, 38 (2007) 745-751.
[41] Y. Liu, H. Xiang, Journal of alloys and compounds, 270 (1998) 154-159.
[42] H. Sehitoglu, I. Karaman, R. Anderson, X. Zhang, K. Gall, H. Maier, Y. Chumlyakov, Acta Materialia, 48 (2000) 3311-3326.
[43] J. Dadda, H. Maier, I. Karaman, H. Karaca, Y. Chumlyakov, Int J Mater Res, 101 (2010) 1503-1513.
[44] I. Kireeva, Y.I. Chumlyakov, Z. Pobedennaya, I. Kretinina, E. Cesari, S. Kustov, C. Picornell, J. Pons, I. Karaman, The Physics of Metals and Metallography, 110 (2010) 78-90.
[45] J. Cui, Y.S. Chu, O.O. Famodu, Y. Furuya, J. Hattrick-Simpers, R.D. James, A. Ludwig, S. Thienhaus, M. Wuttig, Z. Zhang, Nature materials, 5 (2006) 286-290.
[46] C. Picornell, J. Pons, E. Cesari, Scripta materialia, 54 (2006) 459-463.
[47] H. Sehitoglu, J. Jun, X. Zhang, I. Karaman, Y. Chumlyakov, H. Maier, K. Gall, Acta Materialia, 49 (2001) 3609-3620.
[48] R.D. James, K.F. Hane, Acta materialia, 48 (2000) 197-222.
[49] H. Sehitoglu, R. Hamilton, D. Canadinc, X. Zhang, K. Gall, I. Karaman, Y. Chumlyakov, H. Maier, Metallurgical and Materials Transactions A, 34 (2003) 5-13.

Highlights:

- Shape memory and superelastic behaviors of single crystal $Co_{35}Ni_{35}Al_{30}$ alloys have been explored under compression.
- Decrease of recoverable strain with stress was discovered along [100] and [110] orientations.
- CoNiAl demonstrates two-way shape memory effect with narrow thermal hysteresis after thermal cycling experiments.
- Phase diagram of CoNiAl shows a wide range of superelastic window